

pubs.acs.org/JPCB Article

# Shape of AOT Reverse Micelles: The Mesoscopic Assembly Is More Than the Sum of the Parts

Published as part of The Journal of Physical Chemistry B virtual special issue "Mark Ediger Festschrift". Christopher D. Gale,\* Mortaza Derakhshani-Molayousefi,\* and Nancy E. Levinger\*

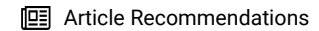


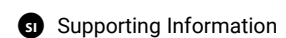
Cite This: J. Phys. Chem. B 2024, 128, 6410-6421



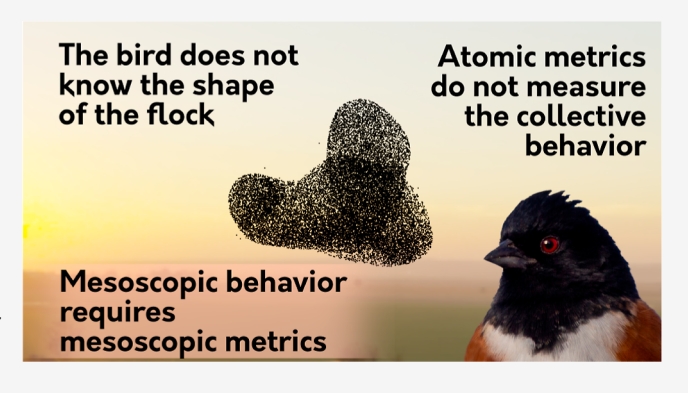
**ACCESS** I







ABSTRACT: AOT reverse micelles are a common and convenient model system for studying the effects of nanoconfinement on aqueous solutions. The reverse micelle shape is important to understanding how the constituent components come together to form the coherent whole and the unique properties observed there. The shape of reverse micelles impacts the amount of interface present and the distance of the solute from the interface and is therefore vital to understanding interfacial properties and the behavior of solutes in the polar core. In this work, we use previously introduced measures of shape, the coordinate-pair eccentricity (CPE) and convexity, and apply them to a series of simulations of AOT reverse micelles. We simulate the most commonly used force field for AOT reverse micelles, the



CHARMM force field, but we also adapt the OPLS force field for use with AOT, the first work to do so, in addition to using both 3- and 4-site water models. Altogether, these simulations are designed to examine the impact of the force field on the shape of the reverse micelles in detail. We also study the time autocorrelation of shape, the water rotational anisotropy decay, and how the CPE changes between the water pool and AOT tail groups. We find that although the force field changes the shape noticeably, AOT reverse micelles are always amorphous particles. The shape of the micelles changes on the order of 10 ns. The water rotational dynamics observed match the experiment and demonstrate slower dynamics relative to bulk water, suggesting a two-population model that fits a core/shell hypothesis. Taken together, our results indicate that it is likely not possible to create a perfect force field that can reproduce every aspect of the AOT reverse micelle accurately. However, the magnitude of the differences between simulations appears relatively small, suggesting that any reasonably derived force field should provide an acceptable model for most work on AOT reverse micelles.

#### 1. INTRODUCTION

Aerosol-OT (AOT) has long been used to study water in nanoconfinement. AOT produces highly consistent reverse micelles approximately 1–10 nm in diameter. At sizes this small, there is a countable number of water molecules inside, allowing scientists an opportunity to study how the properties of water change in the intermediate regime between the microscopic and the macroscopic. The properties of water shift inside the nanoconfinement, sometimes quite dramatically. For instance, previous results show a size-dependent drop in both rotational and translation water motion, and even the hydrogen exchange with protic solutes in reverse micelles slows down. 2,3 There are also unique spectroscopic signatures seen in nanoconfined water from numerous sources, clearly demonstrating that nanoconfinement is a unique environment with behavior not seen in bulk solutions. 4-11 Several studies have suggested that the solutes inside the nanoconfined water pool are not uniformly distributed but tend to preferentially be observed at the interface. <sup>2,3,12-14</sup> This has led to the general assumption that there are two water populations inside reverse micelles, a core and a shell population, which itself introduces another interesting issue about the behavior of water in nanoconfinement. That is, if the properties of both water and any solutes dissolved within a reverse micelle vary with proximity from the interface, then the shape of the reverse micelle plays a pivotal role in the behavior observed in nanoconfinement. This would be a trivial issue if AOT reverse micelles were spherical, like many past studies have implicitly assumed; 9,15–23 however, allatom molecular dynamics (MD) simulations consistently show

Received: April 19, 2024
Revised: June 3, 2024
Accepted: June 5, 2024
Published: June 20, 2024





that the reverse micelles adopt shapes that are anything other than spherical.  $^{24-31}$ 

Shifting from a spherical to an amorphous model challenges us to shift from qualitative descriptions, like visual observations, to quantitative metrics that provide a direct and reproducible measure of the shape. In our previous work, we introduced a set of three metrics, designed so that ideally each metric is independent of the other metrics and can distinguish between every amorphous shape expected to be observed.<sup>32</sup> These metrics are the coordinate-pair eccentricity (CPE), which characterizes an object based on its moments of inertia and classifies the shape into roughly spherical, oblate, or prolate ellipsoids, the convexity, which characterizes the "roughness" of the surface by comparing the observed shape with its convex hull, and the curvature distribution, which analyzes the distribution of either mean or Gaussian curvature computed over points on a surface. In the work presented here, we enlist CPE and convexity to describe shape, leaving out the curvature distribution because we have previously shown that for AOT reverse micelles, the curvature distribution is largely a function of the CPE and convexity, making the curvature distribution a redundant metric in this particular case.<sup>32</sup>

The study of shape offers unique insights into the complex interactions of reverse micelles. The shape of a self-assembled materials, like a reverse micelle, is essentially a more manageable representation of the configurations, reducing a 3N dimensional space down to just three dimensions—two dimensions for CPE and one for convexity. Therefore, shape is directly tied to the partition function and thermodynamics of the system.<sup>33</sup> But the study of shape measures the distribution of these configurations in a soft material directly, a feat not often possible by more traditional methods. In addition to studying the aggregate equilibrium behavior of the system, we are also interested in the continuing conflict between the shapes directly observed in allatom MD<sup>24–31</sup> and those measured by small-angle scattering experiments. <sup>15–19,22,23</sup> Experiments require simplifying assumptions and average over large numbers of shapes in both time and space, which can readily explain almost any variable shape appearing spherical to the experiment, but the all-atom MD simulations done to date use only a single modern force field: the CHARMM force field. <sup>24–31</sup> Therefore, it is still possible that the amorphous shape predicted by simulations to date is the result of force field bias, leaving the conflict between experiment and simulation technically still open. In this work, we introduce the OPLS force field to the field of AOT reverse micelle simulations and investigate the shape of a set of simulations of AOT reverse micelles designed to test how the force field parameters impact the shape. This lets us determine how robust previous observations of the shape of AOT reverse micelles are and to investigate what the shape teaches about the system and how it assembles.

### 2. METHODS

A series of five reverse micelles were simulated using different force fields. Reverse micelles are typically characterized by a parameter known as  $w_0 = [\mathrm{H_2O}]/[\mathrm{AOT}]$ . All reverse micelles simulated here were set to  $w_0 = 5$ , which has been shown to exhibit the effects of nanoconfinement clearly.<sup>1,9,21</sup> The aggregation number, that is, the number of AOT surfactant molecules per reverse micelle, used in this work was 42. This mimics the numbers provided by the Abel lab, which fit well with the current best experimental estimates for  $w_0 = 5$  reverse micelles.<sup>24,30,32,34,35</sup> The reverse micelle was dissolved in 1500

isooctane molecules. Using the average box dimensions of the simulations, the concentration of AOT in isooctane was ~0.17 M. All starting configurations were packed using PACKMOL.<sup>36</sup> The simulations were performed using the 2019 edition of GROMACS. 37-39 Generally, the system was minimized by the steepest descent to remove overlapping contacts. The system was then equilibrated for a total of 10 ns in the NPT ensemble using a series of heavy-atom position restraints, as described in our previous work<sup>32</sup> and provided in Section S1. This system was designed to heavily bias the system toward spherical geometries to prove that nonspherical geometries are not an artifact of the initial configuration but must reflect equilibrium behavior for the system. Equilibration used the velocity-rescale thermostat<sup>40</sup> and Berendsen barostat<sup>41</sup> with a 2 fs step size. Following this, a production run of 1  $\mu$ s was performed using the velocity-rescale thermostat<sup>40</sup> and Parrinello-Rahman barostat<sup>42,43</sup> with a 2 fs step size, saving the coordinates every 8 ps. To study water dynamics, we created a short, 100 ps extension to the production run, saving the coordinates every 100 fs, with all other parameters kept the same. Both the equilibration and production runs were held at 1 bar and 298 K. All simulations used the particle mesh Ewald scheme for computing electrostatic interactions.44

Each simulation differed in the force field used to model the system. One simulation used the CHARMM36 force field for AOT and isooctane<sup>24,45,46</sup> and the TIP3P water model,<sup>47</sup> the most commonly used parameters for all-atom MD simulations of AOT reverse micelles at present. 24,26-31,48 We created a minor modification to this simulation by using the same force field for AOT and isooctane but using the TIP4P/2005 water model<sup>47,49</sup> to understand how the water model impacts the shape and behavior of the reverse micelle. This simulation is expected to be quite different because CHARMM was specifically parameterized for use with the TIP3P water model.<sup>46</sup> We introduce the OPLS force field to explore how the AOT model impacts the reverse micelle. Currently, no major force field family other than CHARMM models a sulfonatebearing surfactant without modification. We chose the OPLS force field because the majority of the reverse micelle simulation comprises organic molecules. We used literature values to properly simulate the sulfonate group.  $^{50-52}$  The literature values were parameterized for a sulfonate-bearing ionic liquid and linear alkyl sulfonate surfactant so none of the parameters are specific to the AOT molecule.

Without performing an expensive, full parameterization of AOT in the OPLS force field, we instead created two additional simulations that modify the partial charges on all atoms of AOT. Although this does not guarantee that the parameters are accurate, with enough variation, it should at least ensure that the force fields straddle a minimum (with respect to any particular metric), with the additional benefit that these schemes will demonstrate specific parameters' impact on the reverse micelle's behavior, especially the shape. As the work presented here shows, a more rigorous parameterization is not guaranteed to be any better, making this method more than sufficient to address the questions posed in this work. To alter the partial charges, we obtained the molecular orbitals for the AOT anion using a density functional theory calculation. Geometry was optimized at the M06/pc-1 level with a level-shift algorithm to help converge the wave function to a solution using GAMESS.<sup>53</sup> At the optimized geometry, a single-point calculation using M06/pc-2 was performed to produce a final set of orbitals. These orbitals were used to compute the partial charges on every

Table 1. Summary of Reverse Micelle Simulations

name	AOT + solvent model	water model	notes
CHARMM	CHARMM36	TIP3P	
CHARMM-4P	CHARMM36	TIP4P/2005	
OPLS-Std	OPLS	TIP4P/2005	sulfonate values from the literature—charges and intramolecular parameters <sup>a</sup>
			LJ parameters <sup>b</sup>
OPLS-CM5	OPLS	TIP4P/2005	OPLS-Std, with CM5 atomic charges
OPLS-RESP	OPLS	TIP4P/2005	OPLS-Std, with RESP atomic charges
<sup>a</sup> Parameters taken from ref 51. <sup>b</sup> Parameters taken from ref 52.			

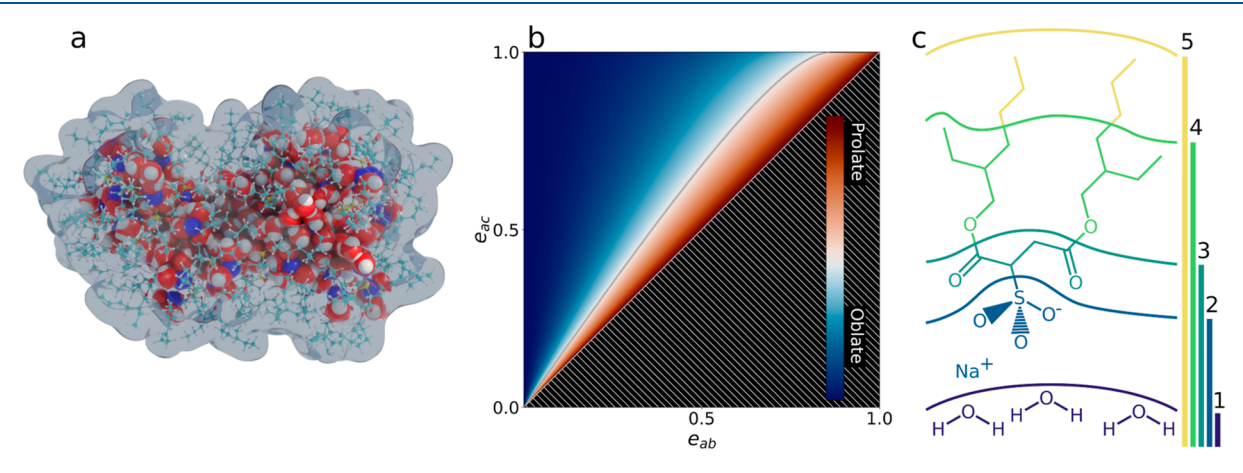


Figure 1. (a) Rendering of the CHARMM simulation reverse micelle illustrating what AOT reverse micelles look like. Water and sodium ions are shown as van der Waals spheres and AOT is shown in a ball-and-stick representation. The glassy surface represents the outer surface of the reverse micelle and is identical to surface 5 in the data presented in this work. (b) Illustration of a CPE plot. The range of CPE has been colored, dividing all possible shapes into either oblate or prolate shapes. (c) Depiction of how the surfaces are defined. Lines on the right illustrate which subset of atoms is included in each surface, as numbered, showing how each subsequent surface includes the previous set as well as the new atoms.

atom of AOT using the *Multiwfn* program.<sup>56</sup> We used both the Hirshfeld-based, CM5 method<sup>57</sup> and the electrostatic potential mapping method, RESP.<sup>58</sup> All simulations employing OPLS-based force fields used the TIP4P/2005 water model.<sup>47,49</sup> Details about the OPLS force fields, including interand intramolecular parameters and partial charges, are provided in Section S2. The different force fields involved and the naming conventions we assign them in this paper are summarized in Table 1.

An example of the aspherical, amorphous shapes exhibited by AOT reverse micelles is shown in Figure 1a. Here, we use CPE and convexity to quantitatively measure these types of shapes. These metrics are described in detail in our previous paper.<sup>32</sup> Briefly, CPE is designed as an extension of eccentricity, which has been used before, <sup>24,28,29</sup> to 3D objects by using a coordinate pair of values. This allows comparison of all three semiaxes of the equivalent ellipsoid and therefore fully characterizes the shape. The semiaxes of the equivalent ellipsoid are traditionally given the variables a, b, and c,  $a \ge b \ge c$ . CPE classifies objects into roughly spherical, oblate-, or prolate-ellipsoidal shapes based on their moments of inertia using two parameters,  $e_{ab}$ , comparing semiaxes a and b, and  $e_{ac}$  comparing semiaxes a and c. An example CPE plot illustrating how the plot divides oblate and prolate shapes is provided in Figure 1b. Oblate ellipsoids are short and fat objects that resemble M&M candies and appear along the left-hand side of a CPE plot, toward the y-axis, shown in blue in Figure 1b. Prolate ellipsoids are long and skinny objects that resemble sausages and appear along the line y = x, shown in red in Figure 1b. We provide a dividing line between more oblate and more prolate regions in all CPE plots because the division is neither linear nor intuitive. Derivation of this

curve appears in Section S3. Spherical objects appear near the origin, and to a good approximation, the radial distance from the origin serves as a measure of the asphericity of the object.

Convexity measures the volume "missing" from the shape, providing a single number that captures the amount divots and folding in the shape. In this work, we define convexity as the volume of the shape divided by the volume of the convex hull of the shape, and we have assigned convexity the variable  $\Xi$ . Convexity has a range  $0 < \Xi \le 1$ . Therefore, a convex shape such as a sphere will have  $\Xi = 1$ , and divots, such as those on a golf ball, or folds, such as a U-shaped object, will reduce the convexity. It is important to recognize that while convexity <1 all but guarantees that there exists a region of negative mean curvature somewhere on the surface so that it may be tempting to equate convexity directly with curvature, these are still separate metrics providing different pieces of information.

For each simulation, the micelle was divided into five surfaces to study how the shape changes between the inner water pool and the oil/surfactant interface. Surfaces are numbered starting from the interior, so that surface 1 corresponds to the shape of the water pool and surface 5 corresponds to the shape of water + Na<sup>+</sup> + AOT. Each surface is created by defining a subset of the atoms in the micelle arranged as nested sets, so that surface 1 is defined as all water molecules, surface 2 is defined as all water plus the sodium plus the sulfonate-group atoms, etc. Figure 1c illustrates how these surfaces work and details where the break points are. To compute CPE, the atoms contained in each surface's subset are used to calculate the moments of inertia directly. To compute convexity, the atoms contained in each surface are used to generate a Willard—Chandler surface that is then used for the analysis. <sup>59</sup> A custom Python code was used for

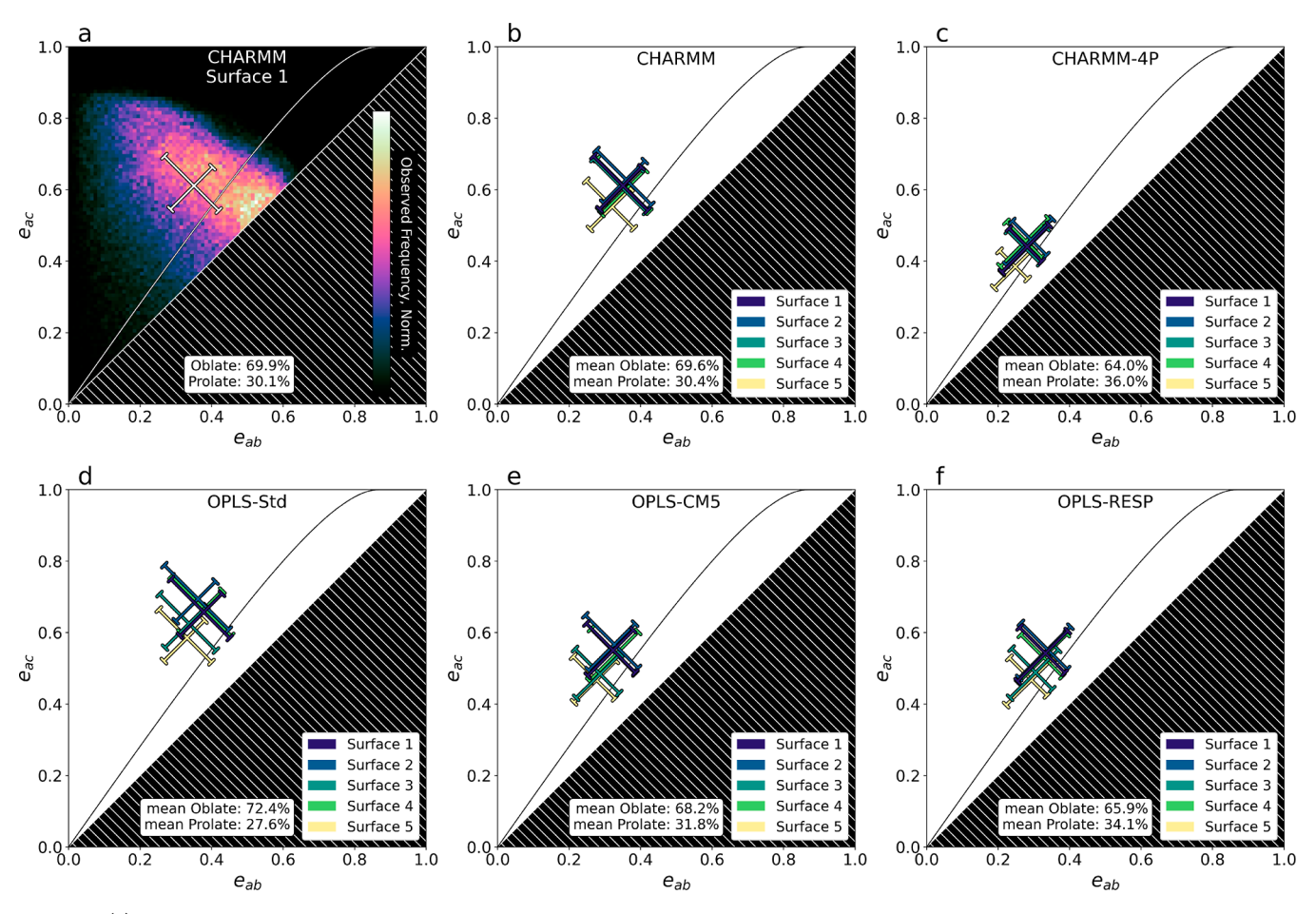


Figure 2. (a) Distribution of CPE values observed over the entire trajectory for the CHARMM simulation, first surface, as a representative sample. Values below the line y = x violate the conventions of CPE and are not observed; we black out this region as a reminder that no data can be observed here. Brighter colors denote a greater number of observations of that value. The cross represents the interquartile range, the cross center represents the median value, and the ends represent the upper and lower quartiles in each dimension. The cross is rotated into the "natural" coordinates by principal component analysis. The curve through the plot represents the dividing line between roughly oblate (left) and prolate (right) shapes. The proportion of the data appearing on each side of the divider is provided at the bottom of the plot. (b-f) Summary of the CPE distributions over the entire trajectory for each surface of each simulation as labeled at the top. Here, the proportions of the time the reverse micelle is either oblate/prolate is given as the mean value over all surfaces.

all analyses,<sup>60</sup> with key packages including the MDAnalysis package for manipulating the simulation trajectory,<sup>61,62</sup> the PyTim package for computing the Willard–Chandler surface,<sup>63</sup> and the PyVista package for manipulating the mesh surfaces.<sup>64</sup>

# 3. RESULTS AND DISCUSSION

**3.1. Coordinate-Pair Eccentricity.** With five simulations each containing five surfaces, displaying the data as a time series is cumbersome, so we present a condensed format, as illustrated in Figure 2a for a representative sample. The heat map in Figure 2a shows the 2D histogram of CPE values computed at every frame in the 1  $\mu$ s simulation. The cross used in Figure 2a represents the multidimensional interquartile range of the data, with the intersection at the median and the ends of the cross representing the lower and upper quartiles, rotated into "natural" coordinates by principal component analysis, and is the method by which the distribution is represented in Figure 2b-f, with each color representing a different surface as labeled in the legend. Heat map plots for each simulation and surface appear in Section S4 for completeness.

The simplest and most notable observation arising from Figure 2b-f is that none of the simulated reverse micelles are

truly spherical. Many experiments and models for AOT reverse micelles have assumed that AOT reverse micelles are spherical. <sup>9,12,20,65,66</sup> However, the work presented here demonstrates consistently, across many different parameter sets, that AOT reverse micelles are significantly aspherical. More specifically, the reverse micelles are typically more oblate than prolate ellipsoidal, although the reverse micelles explore almost all of the space at various points in time.

To aid in the comparison between different simulations, we plot the average CPE behavior over all surfaces of each simulation together in Figure 3. We want to emphasize the comparison between simulations, so the center of each circle accurately represents the median averaged over all surfaces, but the extent of the circle only approximates the average of the interquartile range over all surfaces. Figure 3 reveals natural groupings between our simulations: a "generic" group consisting of CHARMM and OPLS-Std that is also the most highly eccentric group; an "AOT-specific" group including OPLS-CMS and OPLS-RESP that has a lower CPE than the generic group and is therefore relatively more spherical, although still eccentric overall. Finally, the CHARMM-4P simulation stands alone as the most spherical of all the simulations. Given that CHARMM was designed for use with TIP3P water, <sup>46</sup> this simulation is

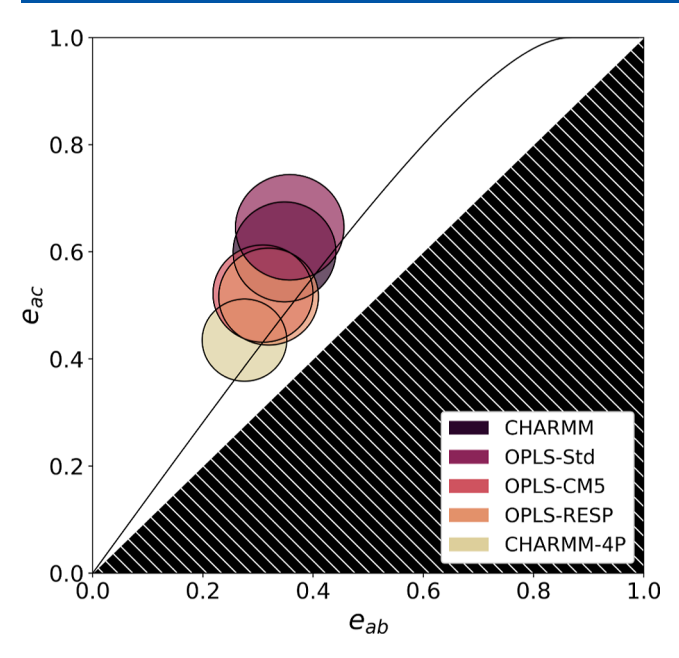


**Figure 3.** Direct comparison of the average behavior of all surfaces for each simulation. The center of each circle represents the mean of the medians of the CPE distribution for each surface, while the radius is roughly equal to the median of the interquartile range for each surface.

unlikely to accurately capture the interaction between the AOT headgroups and water. Although the CHARMM-4P simulation may not represent reality well, it clearly demonstrates that the water/AOT interaction plays an important role in the shape. Based on the magnitude of the difference compared to the differences observed between other simulations, the water/AOT interaction may even be the most important factor impacting the shape.

However, these results also emphasize that the nonspherical shape observed in previous studies<sup>24-31</sup> is highly robust. As Figure 3 demonstrates, although the shape may change slightly with different force fields and simulation parameters, it is always nonspherical. This strongly supports the hypothesis that AOT reverse micelles are aspherical in experiment as well as in simulation because it suggests that the force field cannot explain the discrepancy between experiment and simulation. The only remaining explanation for the difference between experiment and simulation is an artifact of MD simulation itself or an averaging mechanism in small-angle scattering experiments. While we will not examine the effect of MD simulation itself on the shape of AOT reverse micelles, it is unclear how classical mechanics or a periodic boundary would cause an otherwise spherical shape to become aspherical. On the other hand, there is no question that scattering experiments involve significant amounts of ensemble averaging. So, we believe that this is strong evidence that AOT reverse micelles are aspherical and devote the rest of the paper to characterizing this aspherical shape.

The similarity between the simulations that used the appropriate water model designed for use with their respective force fields suggests that any simulation with the appropriate water model produces a reasonably accurate representation of reverse micelles, but it is unexpected that the simulations split into the generic and AOT-specific groups like we observe. The generic group includes CHARMM and OPLS-Std, two force fields developed in different ways for different purposes that we expect would lead to different atomic pairwise interactions. The water/AOT radial distribution functions (RDFs), shown in

Section \$10, indicate that some of the largest differences exist between CHARMM and OPLS-Std. Nevertheless, Figures 2 and 3 show that these force fields result in roughly the same shapes. Similarly, the AOT-specific group includes OPLS-CM5 and OPLS-RESP, two force fields based on DFT calculations but whose specific charges are calculated by very different methods, resulting in very different partial charges for AOT. And yet, Figures 2 and 3 show that these two force fields lead to significantly similar shapes that are also different from the generic group simulations. We made no changes to the Lennard-Jones parameters of AOT to create the OPLS-CM5 and OPLS-RESP force fields, so it is possible that the lower average CPE for the AOT-specific group is a consequence of changing the intermolecular interactions, which are a combination of Lennard-Jones interactions and electrostatic interactions. However, the exact charges on each atom in the CM5 and RESP charge schemes are quite different. If the differences we observe in Figures 2 and 3 were due to a simple mismatch between the electrostatic and Lennard-Jones parameters resulting in incorrect interaction energies between atom pairs, then we expect that the OPLS-CM5 and OPLS-RESP simulations would differ from each other while also differing from the generic group. For example, compared to the sulfonate group charges in the OPLS-Std force field, the CM5 charge scheme has a significantly lower S-O bond dipole, while the RESP charge scheme has a slightly larger S-O bond dipole; if differences like these explained the change in CPE, then OPLS-CM5 and OPLS-RESP should move in opposite directions relative to the OPLS-Std simulation. Instead, both the OPLS-CM5 and OPLS-RESP simulations have nearly identical CPE distributions and, hence, shapes. Additionally, as we show throughout the rest of the paper, our results generally suggest that individual atomic interactions are unlikely to significantly influence the shape. An alternative theory posits that the overall AOT charge distribution—i.e., its dipole, quadrupole, and generally the multipolar expansion—has some importance to accurately modeling the behavior of AOT reverse micelles. Current experiments cannot differentiate the large differences between the CPE values we observe in simulation and a perfect sphere, so we cannot gauge which simulated shapes are more accurate. Nevertheless, the results we present here demonstrate which parameters are important with respect to the shape of AOT reverse micelles.

3.1.1. Investigating the Change in CPE and an Anomaly. In our previous work, we built a model that predicts how the CPE of an arbitrary shape changes with added thickness, in the same way the shape is expected to change from surface 1 to surface 5. Figure 2 shows a notable difference in shape between the inner and outer surfaces of the reverse micelle; specifically, surface 5 shows a noticeable drop in both dimensions of CPE. This indicates that although the outer surface is still not spherical, it is relatively more spherical than the inner shell. This is consistent with the model we created in the previous work and suggests that this difference is mostly the result of the geometry of the system. In fact, if we were to make the tail groups of AOT long and therefore increase the effective distance between surfaces 1 and 5, we would expect the magnitude of the drop in CPE to increase.

Geometry does not completely explain the observed CPE distributions though. In general, across all simulations, there is not a smooth progression from a relatively higher to relatively lower CPE as the surfaces increase, as one would expect if geometry alone explained the data.<sup>67</sup> Instead, for all of the OPLS

simulations (OPLS-Std, OPLS-RESP, and OPLS-CMS), we observe a "back-and-forth" behavior where surfaces 1 and 2 have higher CPE, surface 5 has low CPE, and surfaces 3 and 4 oscillate between high and low CPE. For the CHARMM simulations, we observe no oscillation, but surfaces 1—4 have nearly identical CPE before a large jump in CPE at surface 5. These results may be due to our choice in surfaces. Other than surfaces 1 and 5, representing the water pool and entire reverse micelle, respectively, the choices for surfaces 2—4 and even the number of surfaces analyzed are arbitrary. There is no general understanding of how shape is expected to change throughout the reverse micelle, so we chose several surfaces in the hopes of capturing whatever behavior is present. However, this result may indicate that we selected too many surfaces and are effectively observing noise as the configuration of AOT fluctuates.

We can analyze the changes in CPE in more detail by focusing on  $\triangle$ CPE, which we define as the usual vector difference in CPE, surface 5 minus surface 1. Our model predicts that shapes should generally become more spherical as a shell around the shape becomes larger, corresponding to a  $\Delta$ CPE in the third quadrant, e.g.,  $\triangle CPE = (-, -)$ . We also found that real shapes encountered in chemistry do not always obey our relatively simple model but determine that those points violating our model should be roughly equally distributed between all four quadrants. However, our simulations all show an anomalous number of points in the fourth quadrant, which we could not previously explain. The  $\Delta$ CPE distributions for all simulations are shown in Section S5. The fact that our model cannot explain why the fourth quadrant has a significantly larger portion of the population than the first or second quadrants suggests that our model and geometry alone cannot entirely explain this particular aspect of the shape of AOT reverse micelles, and so, we turn our attention to this anomaly in the hopes of uncovering the chemical reason for this observation. For brevity, much of our analysis on this subject has been moved to the Supporting Information.

We identified a strong propensity for the frames displaying this anomaly to adopt an oblate rather than prolate shape, as illustrated in Section S11. We tested whether a curvature-related reason could account for this anomaly, perhaps due to an energy penalty associated with highly curved interfaces such as those occurring around the sides of an obolate ellipsoid, but did not find evidence to support this idea. These results are presented in Section S11.1. We also tested whether the various surfaces are unrelated to each other by measuring the twist between the principal moments of inertia vector bases of surfaces 1 and 5, shown in Section S11.2. Once again, we found no evidence to support this idea. However, this proves conclusively what we previously took for granted: that the shapes of the reverse micelle at different surfaces are, indeed, connected.

Therefore, we support a more probabilistic view of this phenomenon in which the outer surface adopts a relatively more prolate and spherical shape simply because it is a more likely shape. We note that the median CPE values for all surfaces and all simulations, per Figure 2, are very near to the oblate/prolate divider line. The median values are the most likely values to observe, so the outer surface is simply more likely to look like the median values. This is supported by the fact that although Figure S14 in the Supporting Information shows that it is more likely to be oblate ellipsoidal, this is not an all or nothing situation, and all sorts of shapes are observed with  $\Delta \text{CPE}$  values in the anomalous fourth quadrant. For highly prolate ellipsoids, a tendency to move to the most probable shape is a movement down and to

the left in CPE, a vector in the third quadrant of  $\Delta$ CPE, where our model predicts that most shapes'  $\Delta$ CPE appear. Therefore, although the movement to the most probably shape for an oblate ellipsoid is notable and apparently anomalous, the analogous prolate behavior is also present and simply blends in with the expected behavior.

**3.2. Convexity.** The convexity distribution for each AOT reverse micelle simulation at each surface is shown in Figure 4.

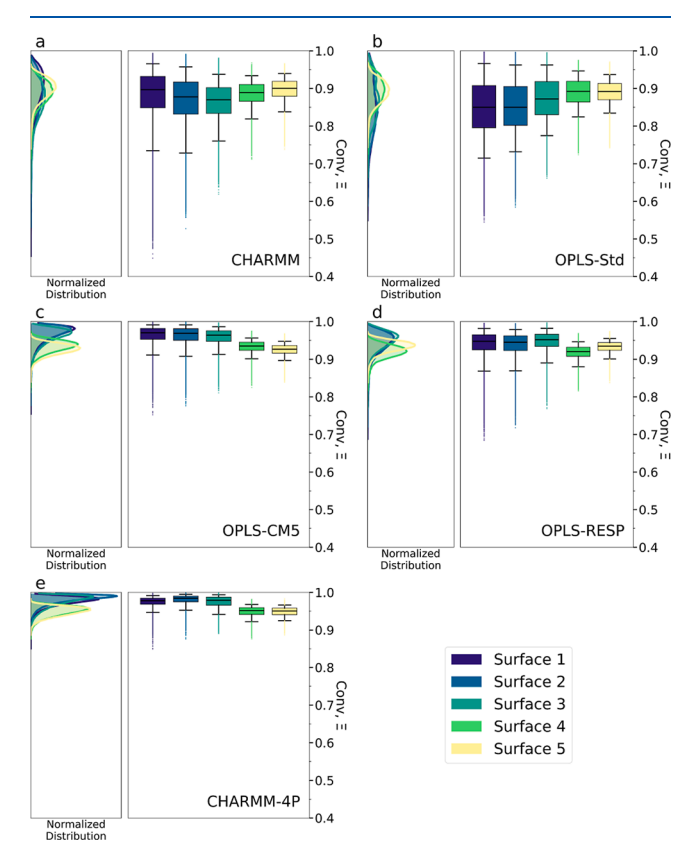


**Figure 4.** (a—e) Convexity distributions for each simulation. The left plots in each panel for each simulation show the smoothed histogram of observed convexity values, while the right plots in each panel provide a box-and-whisker representation of the convexity distribution, where the center line represents the median, the box represents the interquartile range, and the whiskers encompass 95% of the data, with the remaining 5% considered outliers and plotted as individual points.

The distributions on the left and right side of each panel represent the same data, presented in two different ways. The left side shows a natural representation of the distribution as a smoothed histogram, while the right side provides a numerical, box-and-whisker representation. We observe the same general groupings of simulations as with CPE, where Figure 4a,b shows that convexity varies most and has the lowest median values for the generic group simulations. Figure 4c,d shows that the AOT-specific group simulations have slightly narrower distributions with higher median convexity values, and Figure 4e shows that CHARMM-4P has an exceptionally narrow convexity distribution with an exceptionally high median convexity.

Most studies of AOT reverse micelles, and similar objects, use eccentricity as the only measure of shape, implicitly assuming that the CPE, or generally the eccentricity, is the primary indicator of shape changes, a view that we believe should be revised in the future. Consider the CHARMM-4P simulation, where we observe a highly spherical reverse micelle that is also

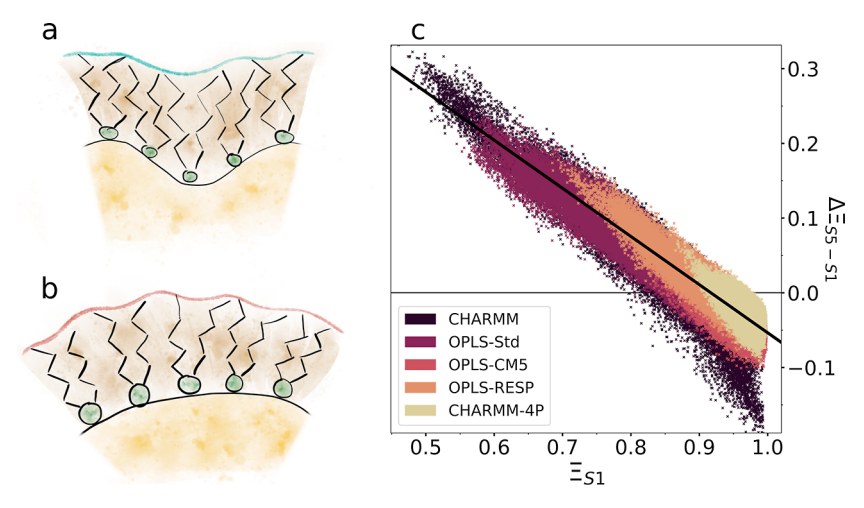


**Figure 5.** (a) Illustration of the low convexity case. The lower, gold portion represents the water pool and green dots with twin tails represent the AOT surfactant. (b) Illustration of the high convexity case, colored the same as in part (a). (c) Plot of the difference in convexity between surface 5 and surface 1 as a function of the convexity of surface 1. The black line represents the orthogonal distance regression linear fit to all simulations.

highly convex. This builds a picture of a pool of water contained within a relatively stiff interface. If we assume that the perturbations causing the shape to change are similar between simulations, then the same perturbations that lead to significant changes in the convexity in the other simulations cause almost no changes in the CHARMM-4P simulation. This suggests that the primary difference between the CHARMM-4P simulation and the other simulations in terms of shape is the stiffness of the interface, e.g., the surface tension, but it also suggests that the convexity might be the "primary" metric of shape, meaning that the CPE changes because the convexity changes and not vice versa. Taken together, these two points suggest that there is a close relationship between convexity and the surface tension. For simulations, this is an attractive possibility because exact computation of the surface tension for a topological ball is a difficult process. The standard methods for calculating the surface tension either utilize a rectangular box and a flat interface,<sup>68</sup> or use a known, generally spherical geometry and apply a known force to measure the deformation.<sup>69</sup> Neither of these options works well for highly curved and amorphous interfaces like those found in AOT reverse micelles. By contrast, computing the convexity is relatively easy and can be performed quickly for any arbitrary surface. A direct relationship between convexity and surface tension could offer an accessible method for determining the surface tension of any topological ball.

Like CPE, convexity also varies among the five surfaces we define for each simulation. Figure 4 shows that the convexity of the outermost surface, surface 5, always has a tighter distribution than the inner surfaces. The range of the convexity as observed by both the upper and lower quartiles and the outliers decreases steadily from surface 1 to 5, across all simulations, regardless of the median of the distribution. Additionally, surface 5 generally has a more "moderate" median value, neither extremely high nor extremely low.

To explain these observed differences in convexity between the surfaces, we propose what we call the "Hedgehog Hypothesis". We consider two cases, one at each extreme. In Figure 5a, we depict the first extreme, where the inner surface has very low convexity and therefore has regions of relatively extreme negative mean curvature. When the reverse micelle has very low convexity, a surfactant normal to the surface would overlap with other surfactant molecules on the opposite side of the divot. Because the overlap is unphysical, instead the surfactants displace in the only direction available to them and fill in the volume of the divot, resulting in a more minor deformation in the outer surface. The outer surface is still most likely not perfectly convex but has a relatively higher convexity than the inner surface. Figure 5b depicts the other extreme, where the reverse micelle is highly convex. In this situation, the surfactants cannot remain closely packed along the entire length of the surfactant, even at the tips, and also cover the entire surface. Geometry dictates that radially arranged spikes around a closed surface, like spokes on a wheel, must diverge and introduce gaps in the outer surface. Therefore, small divots develop in the outer surface that are not present on the inner surface and the convexity of the outer surface is relatively lower. In equivalent but more commonly used chemistry terms, the solvent-accessible surface area increases not only because the outer surface is physically larger but because solvent molecules can intercalate somewhat between the tail groups.

Figure 5a,b and the hypothesis described so far present a simplified picture, and based on the convexity distributions alone, the Hedgehog Hypothesis is applicable only at the extremes of convexity. We tested the Hedgehog Hypothesis by plotting the difference in convexity between the outer and inner surfaces against the convexity of the inner surface, shown in Figure 5c. The difference is defined as  $\Delta\Xi = \Xi_{SS} - \Xi_{SI}$ , so that positive values indicate that the outer surface is more convex than the inner. The convexity difference between surfaces displays a consistent linear trend that is common to all simulations. We find that the linear trend in Figure 5c matches the Hedgehog Hypothesis exactly with the outer surface comparatively more convex when the inner surface is nonconvex and comparatively less convex when the inner surface is convex. More importantly, Figure 5c demonstrates that the pattern extends beyond the extremes and remains true at more moderate values of convexity as well, demonstrating a far stronger correlation than we could initially discern from the convexity distributions. We have fit the distribution of convexity differences to a single line for all simulations. Fitting each simulation individually makes no substantial difference to the fit, making the difference in convexity between surfaces the only data in this paper where all simulations produce the same result.

Despite major differences in the convexity of each AOT reverse micelle simulation, the pattern in  $\Delta\Xi$  is consistent among them, which implies a universal mechanism independent of the simulation parameters. Based on the Hedgehog Hypothesis and the convexity data presented, it seems likely that the trend observed in Figure 5c is closely related to the surfactant identity. A more rigorous answer would require a series of simulations that change the trend line so that the change in the trend line could be clearly correlated to some dependent variable, which is outside of the scope of this paper. So, we simply note the possibility that a reverse micelle prepared with another surfactant, such as cetyltrimethylammonium bromide (CTAB) or one of the many surfactants tested by Nave et al., 22,65,66,70 might also show a consistent linear trend independent of simulation parameters, but with a different fit than the one we find for AOT here. Further work is needed to confirm this.

**3.3. Shape Dynamics.** Beyond a description of what shapes the AOT reverse micelles adopt, we also explore how the reverse micelle shapes change. The autocorrelations of both CPE and convexity measure how the shape changes with time according to each metric. Because CPE is a pair of values, e.g., a vector, it requires a vector autocorrelation, while the convexity autocorrelation is computed as a scalar autocorrelation. Both autocorrelations are normalized to 1 at  $t_{\rm lag} = 0$ . We fit autocorrelations to the sum of two exponential decays

$$ACF^{i}(t_{lag}) = A_{l}^{i}e^{-t_{lag}/\tau_{l}^{i}} + A_{s}^{i}e^{-t_{lag}/\tau_{s}^{i}} , A_{l}^{i} + A_{s}^{i} = 1$$
(1)

where  $A_l$  and  $A_s$  are the amplitudes for the long and short time components, respectively,  $t_{\rm lag}$  is the lag time, and  $\tau_l$  and  $\tau_s$  are the long and short time constants, respectively. The superscript, i, represents either CPE or convexity. Both autocorrelations are normalized to 1 at  $t_{\rm lag}=0$ . Figure 6 summarizes the results, with Figure 6a,b showing values for the time constants,  $\tau_l$  and  $\tau_s$ , respectively, and Figure 6c presenting the amplitudes for each component. The autocorrelations, fits, and residuals are provided in Section S7.

We attribute the long time decays,  $\tau_l^i$ , shown in Figure 6a, to those larger amplitude, concerted changes in shape and the short time response,  $\tau_s^i$ , shown in Figure 6b, to small, fast, random fluctuations resulting from thermal motion. Thermal motion can create random changes in shape. For example, random twisting of the AOT tail groups can change the CPE and convexity by at least some small amount but overall should represent a minor and fast change to the shape because such motion is random and therefore just as likely to increase as decrease the CPE and convexity for a given configuration.

It appears generally true that  $\tau_l^{\Xi}$  is greater than  $\tau_l^{\text{CPE}}$ , but the magnitude of this difference varies quite a bit. This makes sense in terms of what CPE and convexity measure. The convexity represents the behavior of the entire surface and will not change significantly unless the arrangement of the entire reverse micelle changes. By contrast, the CPE will change if just one of the semiaxes of the rotationally equivalent ellipsoid changes, e.g., it is possible to have a situation where  $\delta a = \delta c = 0$  but  $\delta b \neq 0$ , which causes  $\delta e_{ac} = 0$  but  $\delta e_{ab} \neq 0$ , where  $\delta$  is used to denote the change of the given value between two points in time. So, CPE can change even if only a portion of the reverse micelle changes, while the convexity, as a measure of the entire surface, requires a larger and more concerted change in shape. We also note that the variations in reverse micelle shape observed in the

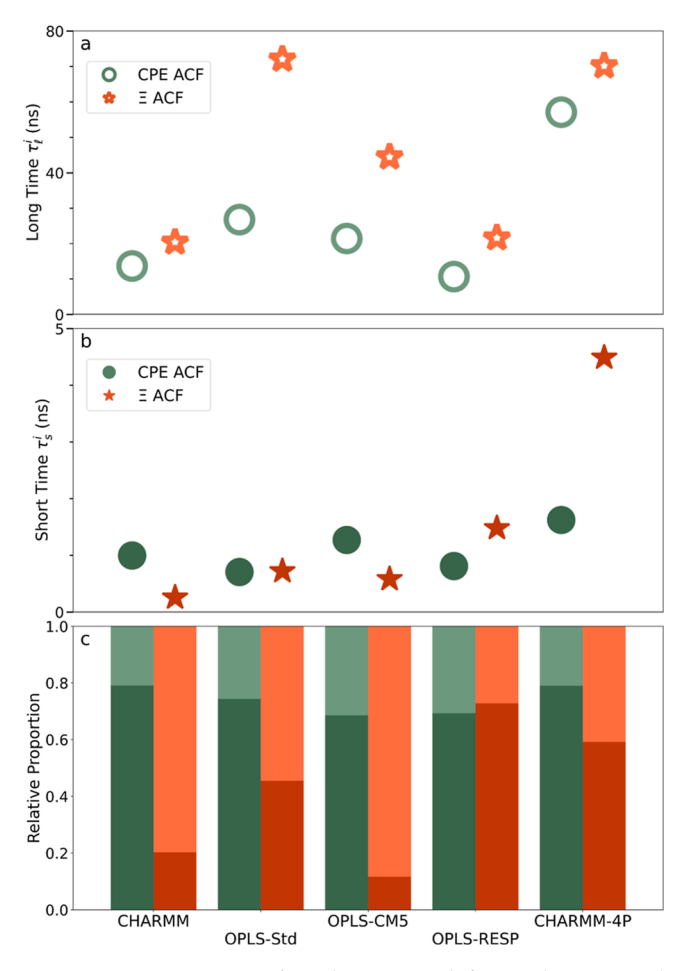


**Figure 6.** Fit parameters from biexponential fits to the CPE and convexity autocorrelations: (a)  $\tau^i_{\rm long}$ , long time constant, (b)  $\tau^i_{\rm short}$  short time constant, and (c) bar graph representation showing how the amplitude is split between the short- and long-time components. The shades of each color match their corresponding time constant; the bottom, darker colored bar corresponds to  $A^i_s$  and the top, lighter colored bar corresponds to  $A^i_l$ .

CHARMM-4P simulations are significantly slower than in almost all of the other simulations; only  $\tau_l^\Xi$  for the OPLS-Std simulation is similar. This is consistent with the hypothesis that the CHARMM-4P reverse micelle has a higher surface tension that damps the shape changes more vigorously and therefore maintains its coherence for significantly longer.

Based on these autocorrelation results, we note that the reverse micelle shape varies on the time scale of tens of nanoseconds, anywhere from 10 to 70 ns depending on the shape metric considered and the model employed. This result places constraints on the experiments and metrics that shape could reasonably impact. For example, water's rotational diffusion occurs on the order of 1 ps, while the fluorescence lifetime of a typical fluorescent probe molecule is on the order of 1 ns. Therefore, we can rule out shape as an important factor in water's rotational diffusion based on the 4 orders of magnitude difference between these two time scales, but we cannot a priori rule out shape as a factor influencing the fluorescence lifetime of a probe molecule placed inside of a reverse micelle. It is still possible that shape has no impact on the fluorescence lifetime of a probe molecule inside of the reverse micelles, but we cannot rule out the possibility that it plays a role without directly studying the role shape plays on the fluorescence lifetime. This

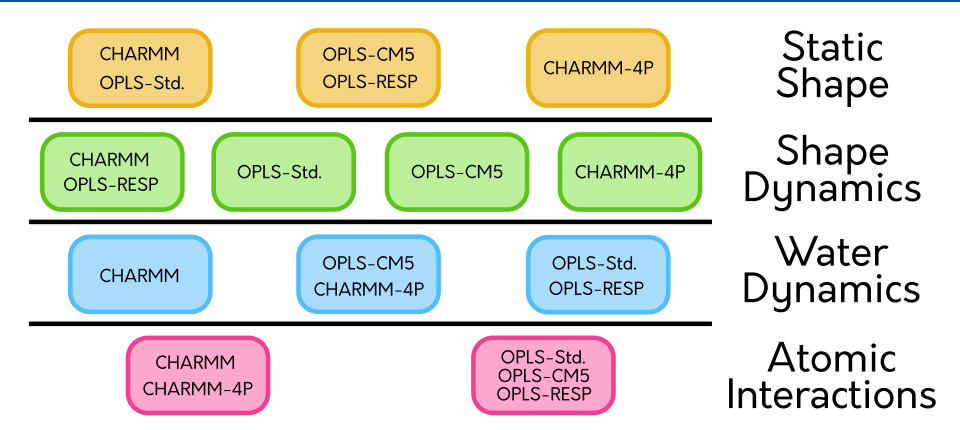


**Figure 7.** Summary of the approximate similarities between simulations across each data type presented in this paper. Static shape refers to both CPE and convexity distributions. Shape dynamics refers to the autocorrelations of CPE and convexity. Water dynamics refers to the rotational anisotropy autocorrelation. Atomic interactions refers to the RDFs, provided in Section S10.

observation could serve as a useful razor, like Occam's razor, to rule out shape as a factor where appropriate and narrow the focus of work to only the processes that shape could reasonably be expected to impact.

**3.4. Other Analyses.** In addition to the analyses already presented, we have also measured several key RDFs as well as the rotational anisotropy decay autocorrelation function of water. While these data complement the results presented here, they are not the main purpose of the paper, so we summarize the results here but provide the data and additional discussion in Sections S8-S10. The water rotational dynamics generally fit expectations based on the past work well. That is, the TIP4P water model exhibits slower dynamics than the TIP3P water model, and the nanoconfinement of the  $w_0 = 5$  reverse micelles studied here exhibit a more complex and slower decay than bulk water. We found that our simulations were best fit by the sum of two stretched exponential decays, with these fits exhibiting predictive power out to longer times even when fit only to the first 10 ns. We believe that this further confirms the core/shell hypothesis proposed previously, although with the added caveat that both homogeneous and heterogeneous broadening is present in the system. 9,71,72 We compared our results to the past work, both simulations<sup>28</sup> and experiments.<sup>9</sup> Martinez et al. simulated slightly different reverse micelles ( $w_0 = 6$ ) but used the CHARMM force field, and our results are in good agreement with their work. The experimental work of Piletic et al., based on pump-probe IR spectroscopy, is limited to examining times  $\leq$ 5.5 ps. As a result, they employ far simpler fits, but our OPLS-RESP and OPLS-Std simulations are in good agreement with their results, suggesting that future work exploring water dynamics in nanoconfinement might be well served by using these force fields over the more traditional CHARMM force field.

The RDFs split exactly down force field lines, regardless of the atom pair examined by the simulation. Despite changing the water model between the CHARMM and CHARMM-4P simulations, the water—AOT sulfonate RDFs and water—sodium ion RDF are virtually identical. There is slightly more variation between the OPLS simulations, but the differences are primarily in the intensity of and shape of the peak, while the peak locations—and therefore mean distances between atoms—are almost entirely unaffected. In all cases, the RDF decays to zero at long distances as the distance, r, becomes larger than the size of the reverse micelle.

# 4. CONCLUSIONS

We created the series of simulations presented here intending to correlate specific simulation parameters and interactions with specific shape effects, but the various results we report present conflicting stories about these parameters. Depending on the simulation parameter, we find different natural groupings, as depicted in Figure 7, which summarizes the patterns seen in each data set. For example, the consistent generic and AOT-specific groups associated with CPE and convexity, as shown in Figures 3 and 4, have no relation to the shape dynamics shown in Figure 6 or to the water dynamics shown in the Supporting Information, Figure S11. And although it is somewhat expected that the force field that governs intermolecular interactions would lead to force field-based patterns in the RDFs in Section S10, patterns among the RDFs also do not correlate well with any of the patterns seen in the other metrics studied in this work.

Reverse micelles are difficult to parameterize as they involve numerous and complicated intermolecular interactions: those between water and AOT, AOT with itself, and AOT with the nonpolar phase. Parameterization involves altering the simulation parameters to recreate one or more experimentally observed quantities. The fact that the simulations do not fall into consistent groups between the several different metrics we present suggests that the metrics involved are largely independent of one another. This makes it hard to find metrics that fully capture all the myriad interactions present in a reverse micelle and all the diverse behaviors we observe in them. This makes it likely that any reverse micelle parameterization effort will only be truly accurate for the narrow aspects on which the system was parameterized. For example, if we could parameterize AOT so that the reverse micelles exactly reproduced an experimentally derived RDF, we cannot expect that simulations using these parameters would reproduce other metrics such as shape, shape dynamics, or water dynamics any more accurately than any other force field; it would only reproduce the RDFs

On the other hand, our results also illustrate that while there are noticeable differences that do not follow clear patterns, there are also universal similarities. In every case, regardless of what force field we used, the shape was measurably aspherical and nonconvex. This highly robust pattern provides strong evidence that AOT reverse micelles are aspherical under almost any conditions, including in real life. This, in turn, suggests that experimental evidence to the contrary is the result of ensemble averaging. Similarly, the time scale for the shape appears to

consistently be on the order of 10 ns regardless of simulation. This provides a useful, generic baseline for determining what processes are most likely unaffected by shape. The robustness of these results also suggests that, for at least some purposes, any force field will be serviceable.

Beyond technical considerations, it is surprising that several of these metrics do not overlap more closely. This may have implications for at least some of the mechanisms governing the behavior within reverse micelles. The observation that the shape and shape dynamics exhibit different groupings suggests that the interactions leading to a particular shape are completely separate from the interactions that determine how that shape changes, even though the shape and its dynamics may seem intimately related. In Section 3.2, we postulated that the convexity is related to the surface tension and the shape is largely a result of random deformations of a loosely bound interface. This implies that the random perturbations responsible for shape vary between the simulations. Unfortunately, it is still unclear whether these random fluctuations are internal or external to the reverse micelle, but the disconnect between the shape and its dynamics implies that the origin of these fluctuations is likely complex.

Although RDFs are extremely helpful, they do not appear to have any particular relation to other aspects of the reverse micelles. The RDFs, shown in Section \$10, fall along force field lines, i.e., the CHARMM simulations are similar, regardless of the water model, and the OPLS simulations are similar, regardless of partial charges. This is not surprising but is worth noting. In chemistry, we often approach the complex, multitiered organization of materials by utilizing either a bottom-up perspective, deriving macroscopic understanding from microscopic behavior, or from a top-down perspective, working backward from macroscopic observables to obtain microscopic understanding. These approaches have been incredibly successful throughout chemistry, taking for example statistical mechanics, a bottom-up approach, and thermodynamics, a top-down approach. However, the disparities between our reverse micelle RDFs, shape, and shape dynamics indicate that a bottom-up microscopic approach is not sufficient to explain the mesoscopic behavior of reverse micelles. Consider that even in our reverse micelles, which include only three components—water, AOT, and isooctane—there are 95 unique atoms leading to 8930 unique two-body interactions, of which an RDF only examines one pair at a time. This number expands exponentially when considering three or more body interactions that are known to be important to accurately modeling chemical systems as simple as pure water. <sup>73,74</sup> It appears as though simple, 2-body interactions may be too reductive to be of much practical use in understanding the mesoscopic behavior of self-assembled AOT reverse micelles.

### ASSOCIATED CONTENT

#### **Data Availability Statement**

The data that support the findings of this study, including the original simulation trajectories, are openly available in Dryad at DOI: 10.5061/dryad.jwstqjqj5.

#### Supporting Information

The Supporting Information is available free of charge at https://pubs.acs.org/doi/10.1021/acs.jpcb.4c02569.

GROMACS style molecular topology files are available on our GitHub page. <sup>60</sup> Equilibrated reverse micelle structure files for each simulation are also provided on our GitHub

page. Program-agnostic tables of parameters used, raw data, fitted values, and some additional analyses (PDF) AOT's structure (PDB)

#### AUTHOR INFORMATION

### **Corresponding Authors**

Christopher D. Gale — Department of Chemistry, Colorado State University, Fort Collins, Colorado 80523, United States; orcid.org/0000-0002-2661-484X; Email: cgale@colostate.edu

Mortaza Derakhshani-Molayousefi — Department of Chemistry, University of Arkansas, Fayetteville, Arkansas 71656, United States; Email: mderakhs@uark.edu

Nancy E. Levinger — Department of Chemistry, Colorado State University, Fort Collins, Colorado 80523, United States; Department of Electrical and Computer Engineering, Colorado State University, Fort Collins, Colorado 80523, United States; orcid.org/0000-0001-9624-4867;

Email: Nancy.Levinger@colostate.edu

Complete contact information is available at: https://pubs.acs.org/10.1021/acs.jpcb.4c02569

#### Notes

The authors declare no competing financial interest.

#### ACKNOWLEDGMENTS

We gratefully acknowledge financial support from Colorado State University and NSF grant 1956323. This work utilized the resources from the University of Colorado Boulder Research Computing Group, which is supported by the National Science Foundation (awards ACI-1532235 and ACI-1532236), the University of Colorado Boulder, and Colorado State University. We thank Grzegorz Szamel and Ana Vila Verde for their helpful comments and productive discussions on the work. We also thank Victor Kiernan for permission to use his excellent photos, including the Spotted Towhee featured in our graphical abstract, photo taken 2 Mar 2024. Victor's work may be found on his Instagram account @victor.kiernan.

# REFERENCES

- (1) Harpham, M. R.; Ladanyi, B. M.; Levinger, N. E.; Herwig, K. W. Water motion in reverse micelles studied by quasielastic neutron scattering and molecular dynamics simulations. *J. Chem. Phys.* **2004**, 121, 7855–7868.
- (2) Wiebenga-Sanford, B. P.; Washington, J. B.; Cosgrove, B.; Palomares, E. F.; Vasquez, D. A.; Rithner, C. D.; Levinger, N. E. Sweet confinement: Glucose and carbohydrate osmolytes in reverse micelles. *J. Phys. Chem. B* **2018**, *122*, 9555–9566.
- (3) Miller, S. L.; Wiebenga-Sanford, B. P.; Rithner, C. D.; Levinger, N. E. Nanoconfinement raises the energy barrier to hydrogen atom exchange between water and glucose. *J. Phys. Chem. B* **2021**, *125*, 3364–3373.
- (4) Boyd, J. E.; Briskman, A.; Colvin, V. L.; Mittleman, D. M. Direct observation of terahertz surface modes in nanometer-sized liquid water pools. *Phys. Rev. Lett.* **2001**, *87*, 147401.
- (5) Venables, D. S.; Huang, K.; Schmuttenmaer, C. A. Effect of reverse micelle size on the librational band of confined water and methanol. *J. Phys. Chem. B* **2001**, *105*, 9132–9138.
- (6) Boyd, J. E.; Briskman, A.; Sayes, C. M.; Mittleman, D.; Colvin, V. Terahertz vibrational modes of inverse micelles. *J. Phys. Chem. B* **2002**, *106*, 6346–6353.
- (7) Zhong, Q.; Steinhurst, D.; Carpenter, E.; Owrutsky, J. Fourier Transform Infrared Spectroscopy of Azide Ion in Reverse Micelles. *Langmuir* **2002**, *18*, 7401–7408.

- (8) Levinger, N. E. Water in confinement. *Science* **2002**, 298, 1722–1723.
- (9) Piletic, I. R.; Moilanen, D. E.; Spry, D. B.; Levinger, N. E.; Fayer, M. D. Testing the core/shell model of nanoconfined water in reverse micelles using linear and nonlinear IR spectroscopy. *J. Phys. Chem. A* **2006**, *110*, 4985–4999.
- (10) Moilanen, D. E.; Levinger, N. E.; Spry, D. B.; Fayer, M. D. Confinement or the nature of the interface? Dynamics of nanoscopic water. *J. Am. Chem. Soc.* **2007**, *129*, 14311–14318.
- (11) Fenn, E. E.; Wong, D. B.; Giammanco, C. H.; Fayer, M. D. Dynamics of water at the interface in reverse micelles: Measurements of spectral diffusion with two-dimensional infrared vibrational echoes. *J. Phys. Chem. B* **2011**, *115*, 11658–11670.
- (12) Baruah, B.; Roden, J. M.; Sedgwick, M.; Correa, N. M.; Crans, D. C.; Levinger, N. E. When is water not water? Exploring water confined in large reverse micelles using a highly charged inorganic molecular probe. *J. Am. Chem. Soc.* **2006**, *128*, 12758–12765.
- (13) Miller, S. L.; Levinger, N. E. Urea Disrupts the AOT Reverse Micelle Structure at Low Temperatures. *Langmuir* **2022**, *38*, 7413–7421.
- (14) Miller, S. L.; Gaidamauskas, E.; Altaf, A. A.; Crans, D. C.; Levinger, N. E. Where Are Sodium Ions in AOT Reverse Micelles? Fluoride Anion Probes Nanoconfined Ions by 19F Nuclear Magnetic Resonance Spectroscopy. *Langmuir* **2023**, *39*, 7811–7819.
- (15) Assih, T.; Larché, F.; Delord, P. Evolution of the radius of the inverse micelles at high dilution in the aerosol-OT/water/n-decane system. *J. Colloid Interface Sci.* **1982**, *89*, 35–39.
- (16) Pileni, M. P.; Zemb, T.; Petit, C. Solubilization by reverse micelles: Solute localization and structure perturbation. *Chem. Phys. Lett.* **1985**, *118*, 414–420.
- (17) Kotlarchyk, M.; Huang, J. S.; Chen, S.-H. Structure of AOT reversed micelles determined by small-angle neutron scattering. *J. Phys. Chem.* **1985**, *89*, 4382–4386.
- (18) Quist, P. O.; Halle, B. Water dynamics and aggregate structure in reversed micelles at sub-zero temperatures. A deuteron spin relaxation study. *J. Chem. Soc. Faraday Trans.* **1988**, *84* (4), 1033–1046.
- (19) Onori, G.; Santucci, A. Viscosity studies of water-containing reversed AOT micelles. *J. Colloid Interface Sci.* **1992**, *150*, 195–199.
- (20) Tomic, M.; Kallay, N. Effect of charge distribution within a droplet on the electrical conductivity of water-in-oil microemulsions. *J. Phys. Chem.* **1992**, *96*, 3874–3882.
- (21) Faeder, J.; Ladanyi, B. M. Molecular dynamics simulations of the interior of aqueous reverse micelles. *J. Phys. Chem. B* **2000**, *104*, 1033–1046.
- (22) Nave, S.; Eastoe, J.; Penfold, J. What is so special about aerosol-OT? Part I. Aqueous systems. *Langmuir* **2000**, *16*, 8733–8740.
- (23) Balakrishnan, S.; Javid, N.; Weingärtner, H.; Winter, R. Smallangle X-ray scattering and near-infrared vibrational spectroscopy of water confined in aerosol-OT reverse micelles. *ChemPhysChem* **2008**, *9*, 2794–2801.
- (24) Abel, S.; Sterpone, F.; Bandyopadhyay, S.; Marchi, M. Molecular modeling and simulations of AOT-water reverse micelles in isooctane: Structural and dynamic properties. *J. Phys. Chem. B* **2004**, *108*, 19458—19466.
- (25) Chowdhary, J.; Ladanyi, B. M. Molecular dynamics simulation of aerosol-OT reverse micelles. *J. Phys. Chem. B* **2009**, *113*, 15029–15039.
- (26) Nevidimov, A. V.; Razumov, V. F. Molecular dynamics simulations of AOT reverse micelles' self-assembly. *Mol. Phys.* **2009**, 107, 2169–2180.
- (27) Vasquez, V. R.; Williams, B. C.; Graeve, O. A. Stability and comparative analysis of AOT/water/isooctane reverse micelle system using dynamic light scattering and molecular dynamics. *J. Phys. Chem. B* **2011**, *115*, 2979–2987.
- (28) Martinez, A. V.; Dominguez, L.; Malolepsza, E.; Moser, A.; Ziegler, Z.; Straub, J. E. Probing the structure and dynamics of confined water in AOT reverse micelles. *J. Phys. Chem. B* **2013**, *117*, 7345–7351.
- (29) Marchi, M.; Abel, S. Modeling the self-aggregation of small AOT reverse micelles from first-principles. *J. Phys. Chem. Lett.* **2015**, *6*, 170–174.

- (30) Eskici, G.; Axelsen, P. H. The size of AOT reverse micelles. *J. Phys. Chem. B* **2016**, *120*, 11337–11347.
- (31) Urano, R.; Pantelopulos, G. A.; Song, S.; Straub, J. E. Characterization of dynamics and mechanism in the self-assembly of AOT reverse micelles. *J. Chem. Phys.* **2018**, *149*, 144901.
- (32) Gale, C. D.; Derakhshani-Molayousefi, M.; Levinger, N. E. How to Characterize Amorphous Shapes: The Tale of a Reverse Micelle. *J. Phys. Chem. B* **2022**, *126*, 953–963.
- (33) Allen, M.; Tildesley, D. Computer Simulation of Liquids, 1st ed.; Oxford University Press: New York, NY, 1987
- (34) Eicke, H.-F.; Rehak, J. On the formation of water/oil-microemulsions. *Helv. Chim. Acta* 1976, 59, 2883–2891.
- (35) Maitra, A. Determination of size parameters of water-aerosol OT-oil reverse micelles from their nuclear magnetic resonance data. *J. Phys. Chem.* **1984**, 88, 5122–5125.
- (36) Martínez, L.; Andrade, R.; Birgin, E. G.; Martínez, J. M. PACKMOL: A package for building initial configurations for molecular dynamics simulations. *J. Comput. Chem.* **2009**, *30*, 2157–2164.
- (37) Berendsen, H. J.; van der Spoel, D.; van Drunen, R. GROMACS: A message-passing parallel molecular dynamics implementation. *Comput. Phys. Commun.* **1995**, *91*, 43–56.
- (38) Van Der Spoel, D.; Lindahl, E.; Hess, B.; Groenhof, G.; Mark, A. E.; Berendsen, H. J. GROMACS: Fast, flexible, and free. *J. Comput. Chem.* **2005**, *26*, 1701–1718.
- (39) Abraham, M. J.; Murtola, T.; Schulz, R.; Páll, S.; Smith, J. C.; Hess, B.; Lindahl, E. GROMACS: High performance molecular simulations through multi-level parallelism from laptops to supercomputers. *SoftwareX* **2015**, *1*–2, 19–25.
- (40) Bussi, G.; Donadio, D.; Parrinello, M. Canonical sampling through velocity rescaling. *J. Chem. Phys.* **2007**, *126*, 014101.
- (41) Berendsen, H. J.; Postma, J. P.; Van Gunsteren, W. F.; Dinola, A.; Haak, J. R. Molecular dynamics with coupling to an external bath. *J. Chem. Phys.* **1984**, *81*, 3684–3690.
- (42) Parrinello, M.; Rahman, A. Polymorphic transitions in single crystals: a new molecular dynamics method. *J. Appl. Phys.* **1981**, *52*, 7182–7190.
- (43) Nosé, S.; Klein, M. Constant pressure molecular dynamics for molecular systems. *Mol. Phys.* **1983**, *50*, 1055–1076.
- (44) Darden, T.; York, D.; Pedersen, L. Particle mesh Ewald: An *N*·log(*N*) method for Ewald sums in large systems. *J. Chem. Phys.* **1993**, 98, 10089–10092.
- (45) Klauda, J. B.; Venable, R. M.; Freites, J. A.; O'Connor, J. W.; Tobias, D. J.; Mondragon-Ramirez, C.; Vorobyov, I.; MacKerell, A. D.; Pastor, R. W. Update of the CHARMM all-atom additive force field for lipids: Validation on six lipid types. *J. Phys. Chem. B* **2010**, *114*, 7830–7843.
- (46) Pastor, R. W.; MacKerell, A. D. Development of the CHARMM force field for lipids. *J. Phys. Chem. Lett.* **2011**, *2*, 1526–1532.
- (47) Jorgensen, W. L.; Chandrasekhar, J.; Madura, J. D.; Impey, R. W.; Klein, M. L. Comparison of simple potential functions for simulating liquid water. *J. Chem. Phys.* **1983**, *79*, 926–935.
- (48) Abel, S. Stéphane Abel's homepage, downloads, equilibrated AOT reverse micelle 2011. http://st-abel.com/downloads.html (accessed 03 20, 2020).
- (49) Abascal, J. L.; Vega, C. A general purpose model for the condensed phases of water: TIP4P/2005. *J. Chem. Phys.* **2005**, *123*, 234505.
- (50) Jorgensen, W. L.; Tirado-Rives, J. The OPLS [optimized potentials for liquid simulations] potential functions for proteins, energy minimizations for crystals of cyclic peptides and crambin. *J. Am. Chem. Soc.* **1988**, *110*, 1657–1666.
- (51) Canongia Lopes, J. N.; Pádua, A. A. H.; Shimizu, K. Molecular force field for ionic liquids IV: Trialkylimidazolium and alkoxycarbonylimidazolium cations; alkylsulfonate and alkylsulfate anions. *J. Phys. Chem. B* **2008**, *112*, 5039–5046.
- (52) Ríos-López, M.; Mendez-Bermúdez, J. G.; Domínguez, H. New force field parameters for the sodium dodecyl sulfate and alpha olefin sulfonate anionic surfactants. *J. Phys. Chem. B* **2018**, 122, 4558–4565.

- (53) Borioni, J. L.; Puiatti, M.; Vera, D. M. A.; Pierini, A. B. In search of the best DFT functional for dealing with organic anionic species. *Phys. Chem. Chem. Phys.* **2017**, *19*, 9189–9198.
- (54) Schmidt, M. W.; Baldridge, K. K.; Boatz, J. A.; Elbert, S. T.; Gordon, M. S.; Jensen, J. H.; Koseki, S.; Matsunaga, N.; Nguyen, K. A.; Su, S.; et al. General atomic and molecular electronic structure system. *J. Comput. Chem.* **1993**, *14*, 1347–1363.
- (55) Gordon, M. S.; Schmidt, M. W. Theory and Applications of Computational Chemistry: the First Forty Years; Dykstra, C. E., Frenking, G., Kim, K. S., Scuseria, G. E., Eds.; Elsevier, 2005; pp 1167–1189.
- (56) Lu, T.; Chen, F. M. Multiwfn: A multifunctional wavefunction analyzer. *J. Comput. Chem.* **2012**, *33*, 580–592.
- (57) Marenich, A. V.; Jerome, S. V.; Cramer, C. J.; Truhlar, D. G. Charge model 5: An extension of Hirshfeld population analysis for the accurate description of molecular interactions in gaseous and condensed phases. J. Chem. Theory Comput. 2012, 8, 527–541.
- (58) Bayly, C. I.; Cieplak, P.; Cornell, W. D.; Kollman, P. A. A well-behaved electrostatic potential based method using charge restraints for deriving atomic charges: The RESP model. *J. Phys. Chem.* **1993**, *97*, 10269–10280.
- (59) Willard, A. P.; Chandler, D. Instantaneous liquid interfaces. J. Phys. Chem. B 2010, 114, 1954–1958.
- (60) Gale, C. D.; Derakhshani-Molayousefi, M.; Levinger, N. E. *How to Think About Shape*, 2022. https://github.com/Levinger-Group/How-to-think-about-Shape (accessed 05 31, 2024).
- (61) Michaud-Agrawal, N.; Denning, E. J.; Woolf, T. B.; Beckstein, O. MDAnalysis: A toolkit for the analysis of molecular dynamics simulations. *J. Comput. Chem.* **2011**, *32*, 2319–2327.
- (62) Gowers, R. J.; Linke, M.; Barnoud, J.; Reddy, T. J.; Melo, M. N.; Seyler, S. L.; Domański, J.; Dotson, D. L.; Buchoux, S.; Kenney, I. M. et al. MDAnalysis: A Python package for the rapid analysis of molecular dynamics simulations. *Proceedings of the 15th Python in Science Conference*, 2016; pp 98–105.
- (63) Sega, M.; Hantal, G.; Fábián, B.; Jedlovszky, P. Pytim: A python package for the interfacial analysis of molecular simulations. *J. Comput. Chem.* **2018**, 39, 2118–2125.
- (64) Sullivan, C.; Kaszynski, A. PyVista: 3D plotting and mesh analysis through a streamlined interface for the Visualization Toolkit (VTK). *J. Open Source Softw.* **2019**, *4*, 1450.
- (65) Nave, S.; Eastoe, J.; Heenan, R. K.; Steytler, D.; Grillo, I. What is so special about aerosol-OT? Part II. Microemulsion systems. *Langmuir* **2000**, *16*, 8741–8748.
- (66) Nave, S.; Eastoe, J.; Heenan, R. K.; Steytler, D.; Grillo, I. What is so special about aerosol-OT? Part III. Glutaconate versus sulfosuccinate headgroups and oil-water interfacial tensions. *Langmuir* **2002**, *18*, 1505–1510.
- (67) Gale, C. D.; Levinger, N. E. Predicting the Geometry of Core-Shell Structures: How a Shape Changes with Constant Added Thickness. *J. Phys. Chem. B* **2024**, *128*, 1317–1324.
- (68) Braga, C.; Smith, E. R.; Nold, A.; Sibley, D. N.; Kalliadasis, S. The pressure tensor across a liquid-vapour interface. *J. Chem. Phys.* **2018**, 149, 044705.
- (69) Sodt, A. J.; Pastor, R. W. The tension of a curved surface from simulation. *J. Chem. Phys.* **2012**, *137*, 234101.
- (70) Nave, S.; Paul, A.; Eastoe, J.; Pitt, A. R.; Heenan, R. K. What is so special about aerosol-OT? Part IV. Phenyl-tipped surfactants. *Langmuir* **2005**, *21*, 10021–10027.
- (71) Berg, M. A.; Darvin, J. R. Measuring a hidden coordinate: Rate-exchange kinetics from 3D correlation functions. *J. Chem. Phys.* **2016**, 145, 054119.
- (72) Berg, M. A.; Kaur, H. Nonparametric analysis of nonexponential and multidimensional kinetics. I. Quantifying rate dispersion, rate heterogeneity, and exchange dynamics. *J. Chem. Phys.* **2017**, *146*, 054104.
- (73) Babin, V.; Medders, G. R.; Paesani, F. Development of a "first principles" water potential with flexible monomers. II: Trimer potential energy surface, third virial coefficient, and small clusters. *J. Chem. Theory Comput.* **2014**, *10*, 1599–1607.

(74) Reddy, S. K.; Straight, S. C.; Bajaj, P.; Huy Pham, C.; Riera, M.; Moberg, D. R.; Morales, M. A.; Knight, C.; Götz, A. W.; Paesani, F. On the accuracy of the MB-pol many-body potential for water: Interaction energies, vibrational frequencies, and classical thermodynamic and dynamical properties from clusters to liquid water and ice. *J. Chem. Phys.* **2016**, *145*, 194504.